Regenerative Therapy 27 (2024) 398–407

Contents lists available at ScienceDirect

Regenerative Therapy

journal homepage: http://www.elsevier.com/locate/reth

Original Article

Adipose-derived stem cells ameliorate radiation-induced lung injury by activating the DDAH1/ADMA/eNOS signaling pathway

Quanwei Fu [a], Qiaohui Gao [a], Shengyuan Jiao [a], Fei Da [a], Juan Guo [a], Yunen Liu [b, c], Junye Liu [a, *]

[a] Department of Radiation Medical Protection, School of Military Preventive Medicine, Air Force Medical University, Xi'an 710038, China
[b] Shenyang Medical College, No. 146, Huanghe North Street, Shenyang 110034, China
[c] Department of Emergency Medicine, General Hospital of Northern Theater Command, No. 83 Road, Shenhe District, Shenyang l10016, China

ARTICLE INFO

Article history:
Received 24 October 2023
Received in revised form
29 March 2024
Accepted 11 April 2024

Keywords:
Adipose-derived stem cells
Radiation exposure
Lung injury
DDAH1/ADMA/eNOS

ABSTRACT

Background: Ionizing radiation-induced lung injury is caused by the initial inflammatory reaction and leads to advanced fibrosis of lung tissue. Adipose-derived stem cells (ASCs) are a type of mesenchymal stem cell that can differentiate into various functional cell types with broad application prospects in the treatment of tissue damage. The purpose of this study was to explore the protective effect of ASCs against radiation-induced lung injury and to provide a novel basis for prevention and treatment of radiation-induced lung injury.

Materials and methods: Fifty mice were randomly divided into a control group (Ctrl), radiation exposure group (IR), radiation exposure plus ASC treatment group (IR + ASC), radiation exposure plus L-257 group (IR + L-257), and radiation exposure plus ASC treatment and L-257 group (IR + ASC + L-257). Mice in IR, IR + ASC, and IR + ASC + L-257 groups were exposed to a single whole-body dose of 5 Gy X-rays (160 kV/25 mA, 1.25 Gy/min). Within 2 h after irradiation, mice in IR + ASC and IR + ASC + L-257 groups were injected with 5×10^6 ASCs via the tail vein. Mice in IR + L-257 and IR + ASC + L-257 groups were intraperitoneally injected with 30 mg/kg L-257 in 0.5 mL saline.

Results: The mice in the IR group exhibited lung hemorrhage, edema, pulmonary fibrosis, and inflammatory cell infiltration, increased release of proinflammatory cytokines, elevation of oxidative stress and apoptosis, and inhibition of the dimethylarginine dimethylamino hydratase 1 (DDAH1)/ADMA/eNOS signaling pathway. ASC treatment alleviated radiation-induced oxidative stress, apoptosis, and inflammation, and restored the DDAH1/ADMA/eNOS signaling pathway. However, L-257 pretreatment offset the protective effect of ASCs against lung inflammation, oxidative stress, and apoptosis.

Conclusions: These data suggest that ASCs ameliorate radiation-induced lung injury, and the mechanism may be mediated through the DDAH1/ADMA/eNOS signaling pathway.

1. Introduction

Radiotherapy plays an important role in cancer treatment as a direct therapy or an adjunct therapy to chemotherapy and surgery. It is also used for palliative therapy to alleviate the symptoms of malignant and non-malignant diseases [1]. However, radiation-induced lung injury is a serious complication of chest radiotherapy. Radiation-induced lung injury includes any pulmonary toxicity caused by radiation therapy, acute radiation pneumonia, and chronic radiation-induced pulmonary fibrosis. Early cell injury leads to cytokine release and recruitment of inflammatory cells, which causes acute pneumonia, and then the body tries to repair the injury, leading to pulmonary fibrosis [2,3]. No controlled study has been conducted to evaluate various therapies for radiation-induced lung injury in humans. Although most studies suggest that systemic glucocorticoids are effective for treatment of radiation-induced lung injury with obvious symptoms, recurrence after the steroid response often occurs [4]. Therefore, treating radiation-induced lung injury reasonably and effectively is an urgent issue to be resolved.

Asymmetric dimethylarginine (ADMA) is a nitric oxide synthase (NOS) inhibitor, and its accumulation is related to the occurrence of

* Corresponding author.
E-mail address: junyeliu@fmmu.edu.cn (J. Liu).
Peer review under responsibility of the Japanese Society for Regenerative Medicine.

https://doi.org/10.1016/j.reth.2024.04.001

hypertension, diabetes, cardiac dysfunction, and lung vessel injury [5–7]. ADMA attenuates endothelial nitric oxide synthase (eNOS) activity to reduce production of nitric oxide (NO) and causes NOS uncoupling to generate free radicals [8]. Dimethylarginine dimethylamino hydratase 1 (DDAH1) plays an essential role in regulating vascular endothelial injury repair and angiogenesis, and is essential to maintain the NO signaling pathway by degrading ADMA [9]. DDAH1 deficiency significantly increases ADMA levels, accelerates cell oxidation, and makes cells more susceptible to apoptosis induced by *tert*-butyl hydroperoxide [10]. Selective DDAH1 inhibitors upregulate ADMA levels in a tissue-specific manner. For example, selective DDAH1 inhibitor L-257 competitively binds to the active site of DDAH1 for isomer-specific competitive inhibition [11]. eNOS is essential to maintain the functions and homeostasis of endothelial cells and regulates pulmonary arterial hypertension [12]. Decreased expression of eNOS makes endothelial cells prone to apoptosis [13]. Therefore, eNOS and eNOS-derived NO are considered to play a role in regulation of vascular functions. However, it is unclear whether the DDAH1/ADMA/eNOS signaling pathway is involved in radiation-induced lung injury.

Adipose-derived stem cells (ASCs), umbilical cord mesenchymal stem cells, and bone marrow mesenchymal stem cells are mesoderm-derived mesenchymal stem cells with the potential for multidirectional differentiation and they secrete various cytokines [14]. ASCs can be easily isolated from liposuction samples and subcutaneous adipose tissue fragments [15]. ASCs play a crucial role in fat formation and angiogenesis, and regulate inflammation and immunity [16]. In addition to potential multidirectional differentiation, ASCs secrete various growth factors, chemokines, and pro-/anti-inflammatory cytokines [17]. The secretion ability of ASCs affects tissue regeneration, angiogenesis, and lymphangiogenesis and inhibits local immune/inflammatory responses and fibrogenesis [18]. Preconditioned ASCs enhance the valve viability of animals with ischemia–reperfusion injury and upregulate the expression of vascular endothelial growth factor (VEGF)-A, TGF-β, and FGF [19]. Furthermore, intraperitoneal injection of ASCs significantly reduces inflammation and improves intestinal re-epithelialization and animal survival [20].

ASCs enhance angiogenesis and adipogenesis-driven tissue regeneration. Moreover, ASCs have anti-apoptotic, anti-fibrosis, antioxidant, and immunomodulatory properties [21], suggesting that ASCs can protect against radiation-induced lung injury. However, it is unclear whether ASCs have a protective effect against lung injury caused by radiation exposure. Therefore, the purpose of this study was to investigate the protective effect of ASCs against radiation-induced lung injury and clarify the possible molecular mechanism.

2. Materials and methods

2.1. Source and characterization of ASCs

The ASCs were provided by the Basic and clinical laboratory of the General Hospital of the Northern Theater Command. This study was approved by the Ethics Committee of Shenyang Military Region General Hospital, Approval No. (2018) 125. Briefly, the fat tissue of healthy patients was repeatedly rinsed with phosphate buffer (PBS) and added with the equivalent volume of 0.1% type I collagenase (KL-X022, Shanghai kanglang Technology Biology Co., Ltd, China), digested in a 37 constant temperature shaking table for 1 h, centrifugated at 300 r/m for 10 min, and supernatant was discarded. 4×10 nucleated cells/cm were inoculated in a 100 mm culture plate and DMEM medium (GIBCO, USA) containing 10% fetal bovine serum (FBS) was added. They were cultured at 37 °C, 5% CO_2 and 100% saturated humidity. The cells were fused to 70%–80%, and the second generation cells were cultured in vitro for detection. The positive markers were CD90, CD44, CD29, CD117, CD13, CD34, CD10, and CD59, while the negative markers were CD31, CD45, CD14, CD34, CD19 and CD56.

2.2. Culture and identification of ASCs

Approximately 15 g of adipose tissue was extracted under aseptic conditions. Red blood cells were removed by washing with PBS. Visible blood vessels in the adipose tissue were removed using ophthalmology scissors. The adipose tissue was cut into small pieces, digested with 0.1% type I collagenase, and centrifuged at 1500 rpm for 10 min. Fat cells and the supernatant were removed. D-Hank's solution was precipitated, passed through a 200-μm mesh, and centrifuged at 1500 rpm for 10 min. Cells were resuspended in high-glucose DMEM containing 15% fetal bovine serum and seeded in sterile culture bottles at an appropriate density. The cells were incubated at 37 °C with 5% CO_2. After 5 days, the medium was changed, and then the medium was changed every 3 days. At 85% confluence, adherent cells were digested with 0.25% trypsin for 3 min. Passaging was carried out at a 1:2 split ratio, and performed again when adherent cells were close to confluency.

Flow cytometry was used to detect specific antigens on passage 3 adipose stem cells. The cells were digested with 0.25% trypsin, centrifuged at 1500 rpm for 10 min, and then incubated at 4 °C for 30 min with FITC-CD37 (FITC-65162, Proteintech, China), PE-CD90 (FBA2067P, RD, China), APC-CD105 (FBA10971A, RD), PerCP-HLA-DR (FBA4869C, RD), PE-Cy7-CD34 (BF00619, RD), and APC-Cy7-CD45 (BF00421, RD). After washing with PBS twice, the antigen-positive rate was determined by 100 μL PBS.

2.3. Animals and experimental groups

A total of 50 male C57BL/6 mice were provided by the Experimental Animal Department of the General Hospital of Northern Theater Command. One week before the experiment, all the mice were kept in an environment of 20–24 °C with a humidity of 55% + 5% and a light/dark cycle of 12/12 h. Ad libitum access to water and food was provided to allow the mice to adopt to the environment. The fifty mice were then randomly and equally divided into control groups (Ctrl), radiation exposure group (IR), radiation exposure plus ASCs treatment group (IR + ASCs), radiation exposure plus L-257 (IR + L-257) and radiation exposure plus ASCs treatment plus L-257 group (IR + ASCs + L-257). The mice in the radiation exposure group and the radiation exposure plus ASCs treatment group were exposed to a single whole-body dose of 5 Gy X-ray (160kV/25 mA, 1.25Gy/min). Within 2 h after irradiation, the mice in the IR + ASCs and IR + ASCs + L-257 groups were injected with 5×10^6 ASCs via the tail vein. Meanwhile, the mice in the IR + L-257 and IR + ASCs + L-257 groups were also injected intraperitoneally 30 mg/kg L-257 in a volume of 0.5 mL saline. For the Ctrl group and IR exposure group, the mice were injected with 0.5 mL saline. The lung samples and serum were collected on the 14th days of the experiment. All animal protocols were approved by the Institutional Animal Care and Use Committee of General Hospital of Northern Theater Command, and all care and handling of animals was in accordance with the criteria outlined by National Institutes of Health guidelines, NO. Y (2020) 089.

2.4. Samples collection and processing

On the 14th day after the experiment, the mice were prone on the operating table and anesthetized intraperitoneally with sodium pentobarbital (2%, 1.5 mL/kg). The serum and lung samples were collected. For histological examination, the left lung was immersed in 10% neutral-buffered formalin and then subjected to histological

staining and observation. The filter paper was first used to dry the upper lobe of the right lung, and the wet weight of the lung was measured with a balance. The upper lobe of the lung was subsequently dried in an oven at 60 °C for 72 h, and the dry weight was recorded. The edema formation was indicated by calculating the wet weight/dry weight (W/D) ratio. The remaining unused lung samples were stored in liquid nitrogen for subsequent protein analysis.

2.5. Enzyme-linked immunosorbent assay (ELISA) detection

The elisa was used to determine the concentrations of the ADMA (F15035, Bio-Swamp Immunoassay R&D Center, Shanghai, China) and NO (F16320, Bio-Swamp Immunoassay R&D Center, Shanghai, China) in the lungs by the elisa according to the manufacturers'instructions. The optical density at 450 nm was used to measure the concentration of ADMA and NO in a microplate reader. To generate the standard curve, plot optical density value versus standard concentration. The curve equation and r value were calculated to determine the concentrations of the samples.

2.6. Histological analysis

The left lung was fixed in 10% neutral-buffered formalin, and then embedded in paraffin by Leica Microsystem tissue processor (ASP 300S, Germany). The paraffin-embedded the lung tissues were subsequently cut into 3–4 μm thick slices using the Leica Microsystem microtome (Model RM 2265, Germany) and stained with hematoxylin and eosin (H&E).

2.7. Masson's trichrome staining

After dewaxing, the sections were washed with water and air dried. The nuclei were stained with the reagent A (Masson's triehrome staining kit, Shanghai Bogu Biotechnology Co., Ltd) for 10 min and showed blue by microscopic examination. After water washing and air drying, they were treated with the reagent B at room temperature for 15 min. After cleaning with the reagent C, add the reagent D for differentiation, and then dye with reagent e for 10 s. After cleaning with the reagent C, it was transparent with 95% alcohol, anhydrous alcohol and xylene, and finally sealed with neutral gum. After dyeing, it was observed under the microscope.

2.8. Detection of reactive oxygen species (ROS)

The level of ROS in the lung samples was determined by staining with 2,3-Dimethoxy-1,4-naphthoquinone (DMNQ, Sigma, USA) at a 1:100 dilution for 15 min. The ROS intensity was observed under a fluorescence microscope (BX43, Olympus, Japan).

2.9. Terminal deoxynucleotidyl transferase dUTP nick end labeling (TUNEL)

The apoptotic cells in the lung were determined using the TUNEL kit (40306ES20, Cloud-Clone Company, USA) according to the manufacturer's instructions. The nuclei stained red are considered to be apoptotic cells. To calculate the apoptotic index, the percentage of apoptotic cells in 5 randomly selected fields under a fluorescent microscope at ×400 magnification was calculated.

2.10. Western blotting

The Western blot was done as described previously [22]. Briefly, the lung samples were immersed in the RIPA lysis buffer containing 1× protease inhibitor cocktail and lysed homogeneously by Sonic Dismembrator 100 (Fisher Scientific, USA). Bio-Rad Protein Assay was used to determine protein concentration. An equal amount of soluble proteins was separated on 10% sodium dodecyl sulfate polyacrylamide gel electrophoresis (SDS-PAGE), and then transferred onto a PVDF membrane. After blocking with 5% nonfat milk in the TBS, the membrane was probed with primary antibody as follows. Antibody against tumor necrosis factor-alpha (TNF-α, ab8348), IL-10 (ab9969), myeloperoxidase (MPO, ab208670) and IREα (ab3294) were purchased from Abcam (UK) at 1:2000 dilution. Antibody against IL-6 (ab9324) and MDA5 (ab69983) were obtained from Abcam at a 1:1000 dilution. Antibody against eNOS (ab199956, Abcam, UK) was used at 1:250 dilution. Interleukin-1β (IL-1β, sc-7884), Bax (sc-526), Bcl-2 (sc-7382), and SOD-1 (sc-11407) were purchased from Santa Cruz Biotechnology (USA) and used at a 1:2000 dilution. Cleaved caspase 3 (sc-7148) from Santa Cruz Biotechnology (USA), DDAH1 (ab180599) and DDAH2 (ab184166) from Abcam (UK), and GAPDH (sc-32233) from Santa Cruz Biotechnology (USA) were used at 1:500, 1:1000, 1:1000 and 1:5000 dilution, respectively. The blotted membranes were then washed twice with TBS containing 0.1% of Tween 20 to remove unbounded primary antibody and then blotted with corresponding horseradish peroxidase-conjugated secondary antibody. The goat anti-rabbit (ab6721, Abcam, UK), and goat anti-rat secondary antibody (ab7097, Abcam, UK) were used at 1:4000, and 1:1500 dilution, respectively. The chemiluminescent signal was visualized using a clarity western ECL substrate, and the signal was imaged by Tanon 5200 imaging system (Tanon Science and Technology, China).

2.11. Statistical analysis

The data were expressed as the means ± standard deviations error (SE) and analyzed using t-tests and one-way ANOVA with Tukey post hoc test. All statistical analyses were carried out using IBM SPSS Statistics (Version 20.0, Armonk, New York, USA). A two-sided $p < 0.05$ was considered statistically significant.

3. Results

3.1. Identification results of ASCs

As shown in Fig. 1A–G, the results of flow cytometry showed that the surface markers of the 3rd generation ASCs were mainly CD37, CD90, CD105, the markers CD34, CD45 and PerCP-HLA-DR were not expressed. As shown in Fig. 1H, oil red O staining showed that there were reddish lipid droplets with different sizes in ASCs cytoplasm.

3.2. ASCs ameliorated radiation exposure-induced lung injury

The lung weight to body weight ratio and the W/D ratio, which is a marker of the severity of the lung injury, and pulmonary edema in the IR group were significantly increased compared with the Ctrl group. Moreover, ASCs significantly reduced the lung weight to body weight ratio and the W/D ratio caused by IR exposure (Fig. 2A–B, $p < 0.05$). Histopathological analysis showed that IR exposure caused the severe lung injury, characterized by apparent hemorrhage, edema, inflammatory cell infiltration, and collagen deposition (Fig. 2C). However, the severe lung injury was significantly ameliorated by ASCs treatment, suggesting that ASCs could effectively ameliorate IR exposure-induced the lung injury.

3.3. ASCs attenuated lung inflammation and fibrosis caused by radiation exposure

Compared with the Ctrl group, the expression levels of IL-1β, MPO and TNF-α in the IR group were significantly increased. In

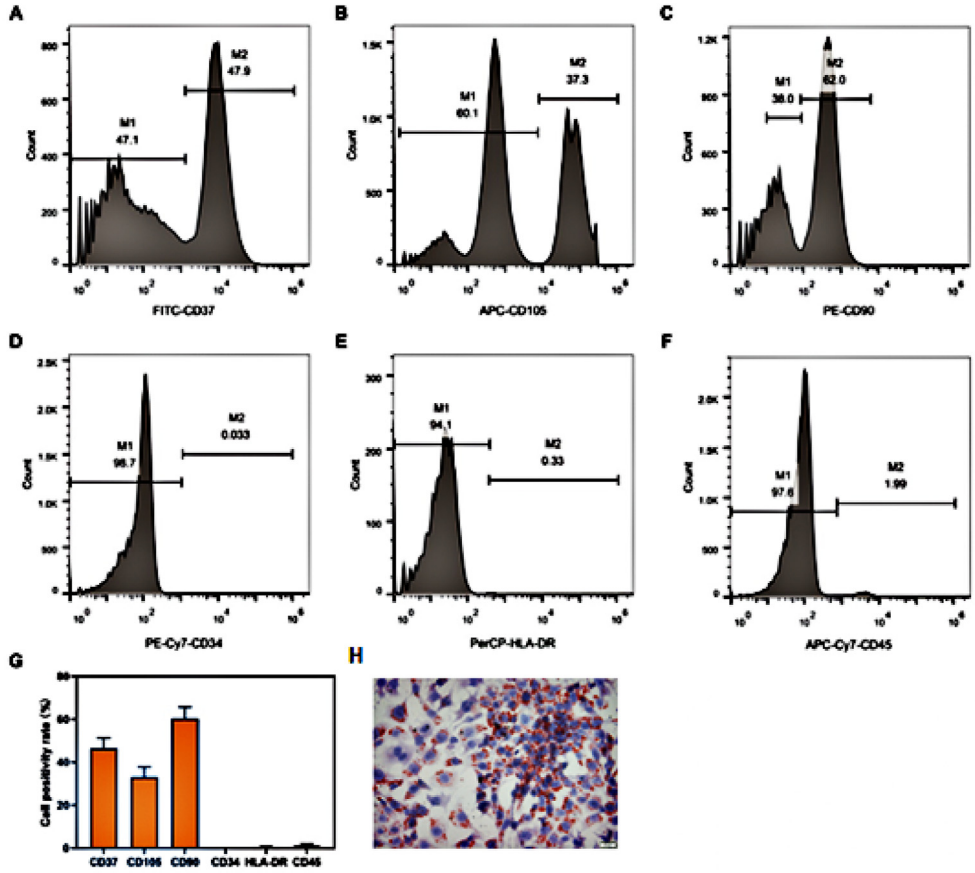

Fig. 1. Identification of surface antigens of adipose-derived mesenchymal stem cells. The flow cytometry results of surface markers of adipose stem cells showed positive expression of CD37, CD90 and CD105; H is the result of oil red O staining after adipogenic differentiation of adipose stem cells.

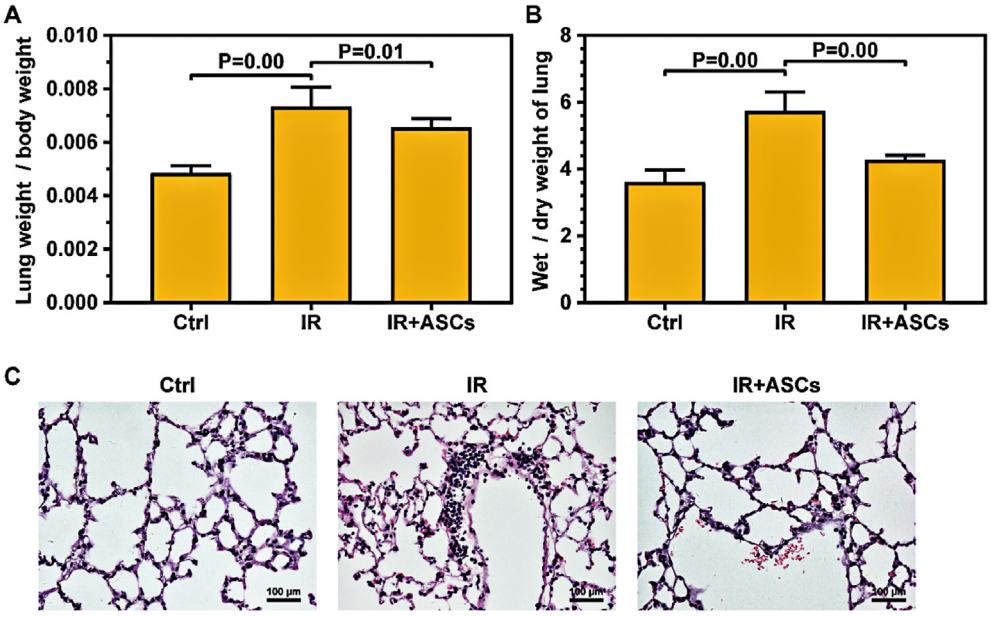

Fig. 2. ASCs ameliorated radiation exposure-induced lung injury. Exposure to IR significantly increased the (A) lung weight to body weight ratio and the (B) W/D ratio of the rats. ASCs treatment significantly reduced the increase in the lung weight to body weight ratio and the W/D ratio caused by IR exposure (A–B). (C) Representative histopathological lung images of rat in the Ctrl group (left panel), IR group (middle panel), and IR + ASCs group (right panel). Scale bar = 100 μm.

contrast, IL-10 expression level greatly decreased. Moreover, ASCs significantly attenuated the elevated levels of TNF-α, MPO, IL-1β, and decreased level of IL-10 caused by IR exposure (Fig. 3A–E, $p < 0.05$). In addition, IR exposure caused obvious collagen deposition and alveolar septal thickening in the lungs, and ASCs treatment significantly reduced collagen deposition (Fig. 3F–G, $p < 0.05$). These data indicate that ASCs can reduce IR exposure-induced inflammation and fibrosis in the lungs.

Fig. S1 (as shown in supporting information) also showed that ASCs improved radiation exposure-induced lung damage, such as AQP-5, SP-A, SP-C, and SP-D, with changes in expression in mice lungs after ASCs treatment.

3.4. ASCs suppressed oxidative stress in the lungs caused by radiation exposure

Compared with the Ctrl group, the IR group had significantly higher ROS levels (Fig. 4A). However, ASCs significantly reduced the elevated ROS levels caused by IR exposure. In addition to increasing ROS levels, IR exposure also significantly increased the expression of IRE-a and MDA5, and decreased the expression of SOD-1. Similarly, ASCs significantly suppressed the increase in IRE-a and MDA5 expression and the decrease in SOD-1 expression caused by IR exposure (Fig. 4B–E, $p < 0.05$). These data showed that ASCs could attenuate IR exposure-induced oxidative stress in the lungs.

3.5. ASCs reduced cell apoptosis in the lungs caused by radiation exposure

The number of apoptotic cells (TUNEL-positive) in the IR group was significantly increased compared with the Ctrl group, and ASCs effectively reduced the increase in the number of apoptotic cells (Fig. 5A–B, $p < 0.05$). In addition, in the IR group, Bax and cleaved caspase-3 expression were significantly increased, and Bcl-2 expression was significantly reduced (Fig. 5C–F, $p < 0.05$). However, ASCs treatment significantly reduced the above effects of the IR exposure, suggesting that ASCs can reduce IR exposure-induced cell apoptosis in the lungs.

3.6. The effects ASCs on DDAH1/ADMA signaling pathway

In order to determine whether the DDAH1/ADMA signaling pathway is involved in the IR exposure-induced the lung injury, the expression levels of DDAH1, DDAH2 and ADMA in the lungs were measured by the elisa and western blotting. Compared with the Ctrl group, the expression level of DDAH1 (the main catabolic enzyme of ADMA) and DDAH2 in the lungs were significantly reduced in the IR group (Fig. 6A–C, $p < 0.05$). In the IR group, the expression of the endogenous eNOS inhibitor ADMA in the lung was significantly increased (Fig. 6D, $p < 0.05$). Moreover, ASCs significantly attenuated the increase in the ADMA expression and the decrease in the DDAH1 and DDAH2 expression caused by the IR exposure.

3.7. ASCs restored eNOS expression and eNOS-derived NO levels caused by radiation exposure

To further explore the possible molecular mechanism of the lung injury caused by IR exposure, the expression of eNOS and eNOS-derived NO were determined by western blotting and elisa. Compared with the Ctrl group, eNOS expression and NO concentration in the lungs were significantly decreased in the IR group,

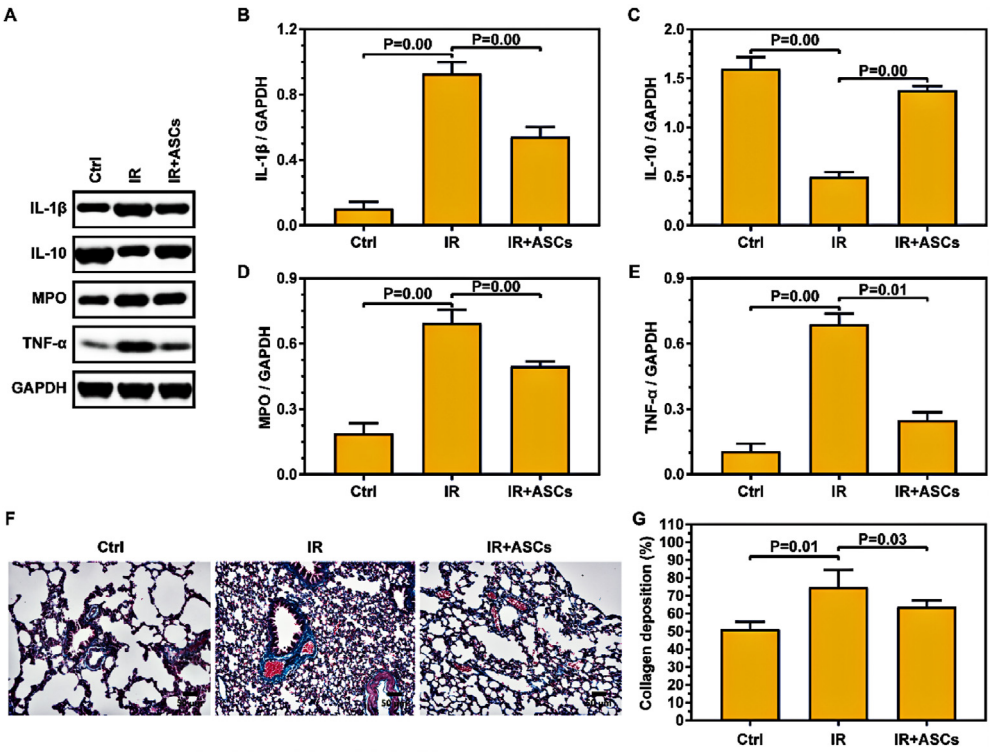

Fig. 3. ASCs attenuated radiation-induced lung inflammation and fibrosis. (A) Representative Western blot images of the expression of IL-1β, IL-10, MPO, TNF-α, and GAPDH. (B–E) Quantitative analysis of the signal density of IL-1β (B), IL-10 (C), MPO (D), and TNF-α (E) with normalized to internal control GAPDH. (F,G) Representative Masson's trichrome staining images and quantitative analysis of collagen deposition. Data are expressed as the mean ± SEM of values obtained from 10 rats in each group. Independent experiments were repeated at least three times. The asterisk and hashtag label indicate statistical significance compared to the Ctrl group and the IR exposure group, respectively. $P < 0.05$ is considered statistically significant.

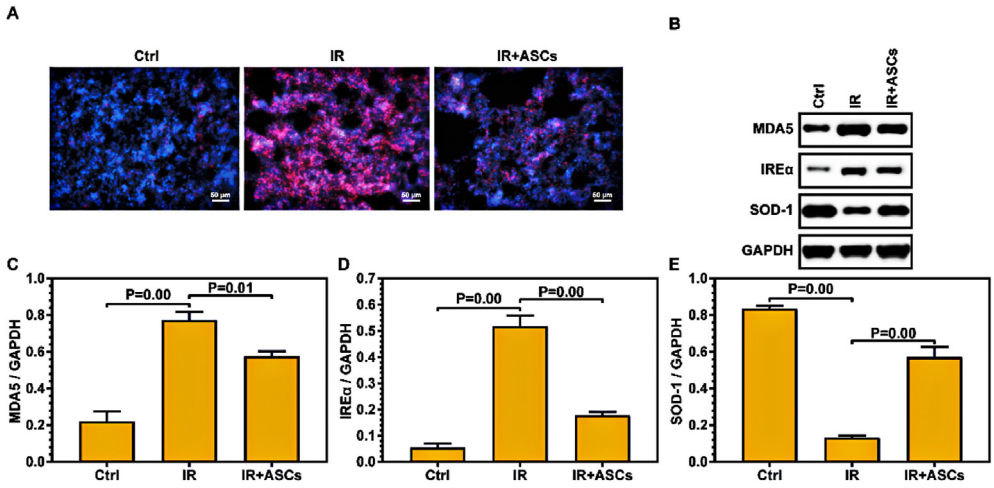

Fig. 4. ASCs suppressed radiation-induced oxidative stress in the lungs. (A) Representative images of intracellular ROS content in the Ctrl group (left panel), IR group (middle panel), and IR + ASCs group (right panel). (B) Representative Western blot images of the expression of MDA5, IREα, SOD-1 and GAPDH. (C–E) Quantitative analysis of the signal intensity of MDA5 (C), IREα (D), and SOD-1 (E) with normalized to internal control GAPDH. Data are expressed as the mean ± SD of values obtained from 10 rats in each group. Independent experiments were repeated at least three times.

whereas ASCs treatment significantly enhanced eNOS expression and NO concentration (Fig. 7, $p < 0.05$).

3.8. L-257 pretreatment offset the protective effect of ASCs on radiation exposure–induced lung injury

To further investigate the mechanism of ASCs on the lung injury caused by IR exposure, L-257, a highly specific competitive inhibitor of DDAH1, was used in this study. Compared with the IR + ASCs group, L-257 pretreatment significantly decreased DDAH1 expression, and increased ADMA expression in the lungs (Fig. 8A–C, $p < 0.05$). Moreover, L-257 pretreatment markedly increased the lung weight/body weight ratio and W/D ratio (Fig. 8D–E, $p < 0.05$), increased hemorrhage, edema and inflammatory cells infiltration in the lungs (Fig. 8F), promoted IL-1β, and TNF-α expression, and reduced IL-10 expression (Fig. 8G–J, $p < 0.05$). Meanwhile, L-257

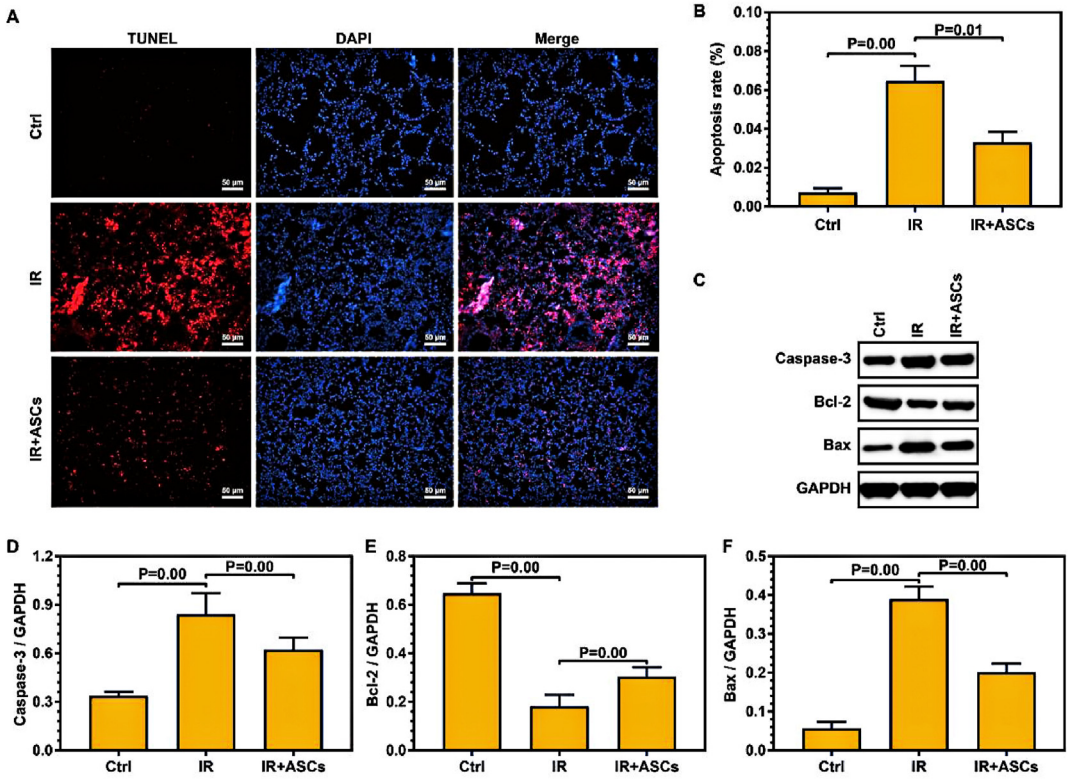

Fig. 5. ASCs alleviated radiation-induced lung cell apoptosis. (A) Representative images and (B) quantitative analysis of apoptotic cells in the lungs by TUNEL staining (Scale bar = 50 μm). (C) Representative Western blot images of the expression of cleave caspase-3, Bcl-2, Bax and GAPDH in each group. (D–F) Quantitative analysis of the signal intensity of caspase-3 (D), Bcl-2 (E), and Bax (F) expression with normalized to internal control GAPDH. Data are expressed as the mean ± SD of values obtained from 10 rats in each group. Independent experiments were repeated at least three times.

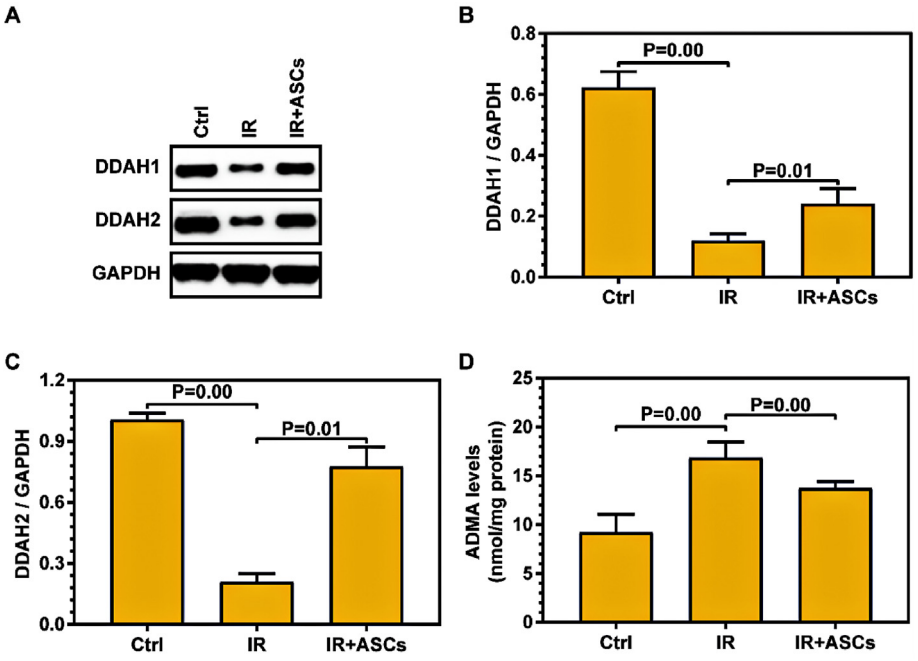

Fig. 6. The effects of ASCs on radiation-induced DDAH1/ADMA signaling pathway. (A) Representative Western blot images of DDAH1, DDAH2 and GAPDH expression in the Ctrl group, IR group, and IR + ASCs group. (B) Quantitative analysis of signal intensity of DDAH1 with normalized to GAPDH. (C) Quantitative analysis of signal intensity of DDAH2 with normalized to GAPDH. (D) ADMA levels in the lung tissues in each group were measured and quantified by ELISA. Data are expressed as the mean ± SD of values obtained from 10 rats in each group. Independent experiments were repeated at least three times. The asterisk and hashtag label indicate statistical significance compared to the Ctrl group and the IR group, respectively. $P < 0.05$ is considered statistically significant.

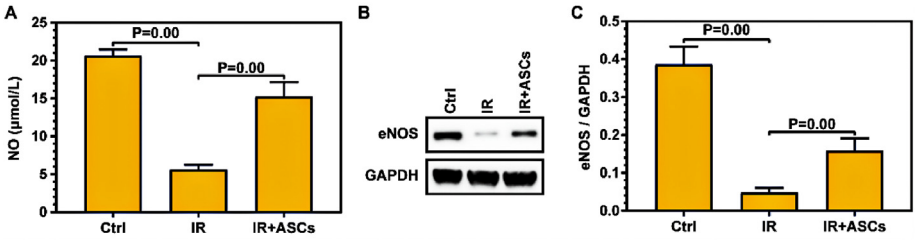

Fig. 7. ASCs enhanced eNOS expression and eNOS-derived NO production in radiation-induced lung injury. (A) The level of NO in each group was determined by ELISA. (B) Representative Western blot images of eNOS and GAPDH in the control group, IR group, and IR + ASCs group. (C) Quantitative analysis of signal intensity of eNOS with normalized to GAPDH in each group.

pretreatment also significantly increased MDA5, IRE-a, Bax and cleave Caspase-3 expression, and decreased SOD-1 and Bcl-2 expression compared with the IR + ASCs group (Fig. 8K–R, $p < 0.05$).

4. Discussion

Radiation-induced lung injury is caused by an early inflammatory response and leads to chronic fibrosis, which is a common complication of chest tumor radiotherapy. The fibrotic process results in the deposition of large amounts of type I and III collagen, which can lead to the proliferation of lung fibrous tissue, destruction of alveolar structures, and impaired lung function [1–5]. In this study, adipose-derived stem cells were used to elicit a therapeutic effect against radiation-induced lung injury in mice. The results showed that adipose-derived stem cell injection had a significant therapeutic effect against radiation-induced lung injury in mice. They attenuated lung inflammation and fibrosis, and inhibited oxidative stress in lungs caused by radiation exposure. The underlying mechanism may be related to promoting the repair of damaged lung tissue by lung stem cells. We investigated the role of the DDAH1/ADMA/eNOS signaling pathway in the inflammatory response to radiation. Activation of the DDAH1/ADMA/eNOS signaling pathway was significantly reduced in the mouse model of radiation-induced lung injury. Pretreatment with L-257, a highly specific competitive inhibitor of DDAH1, counteracted the protective effect of ASCs against lung inflammation, oxidative stress, and apoptosis induced by IR exposure, suggesting that the mechanism may be mediated through the DDAH1/ADMA/eNOS signaling pathway. These results suggest that promoting the DDAH1/ADMA/eNOS signaling pathway is an effective method to prevent and treat radiation-induced lung injury. Our results also revealed several major events in the occurrence and development of radiation-induced lung injury. Moreover, our evidence for preventing and treating radiation-induced lung injury was obtained by regulating these targets, providing an experimental basis to further explore effective methods to prevent and treat radiation-induced lung injury.

ASCs are stem cells with the potential of multidirectional differentiation. They have various sources, are easy to collect with

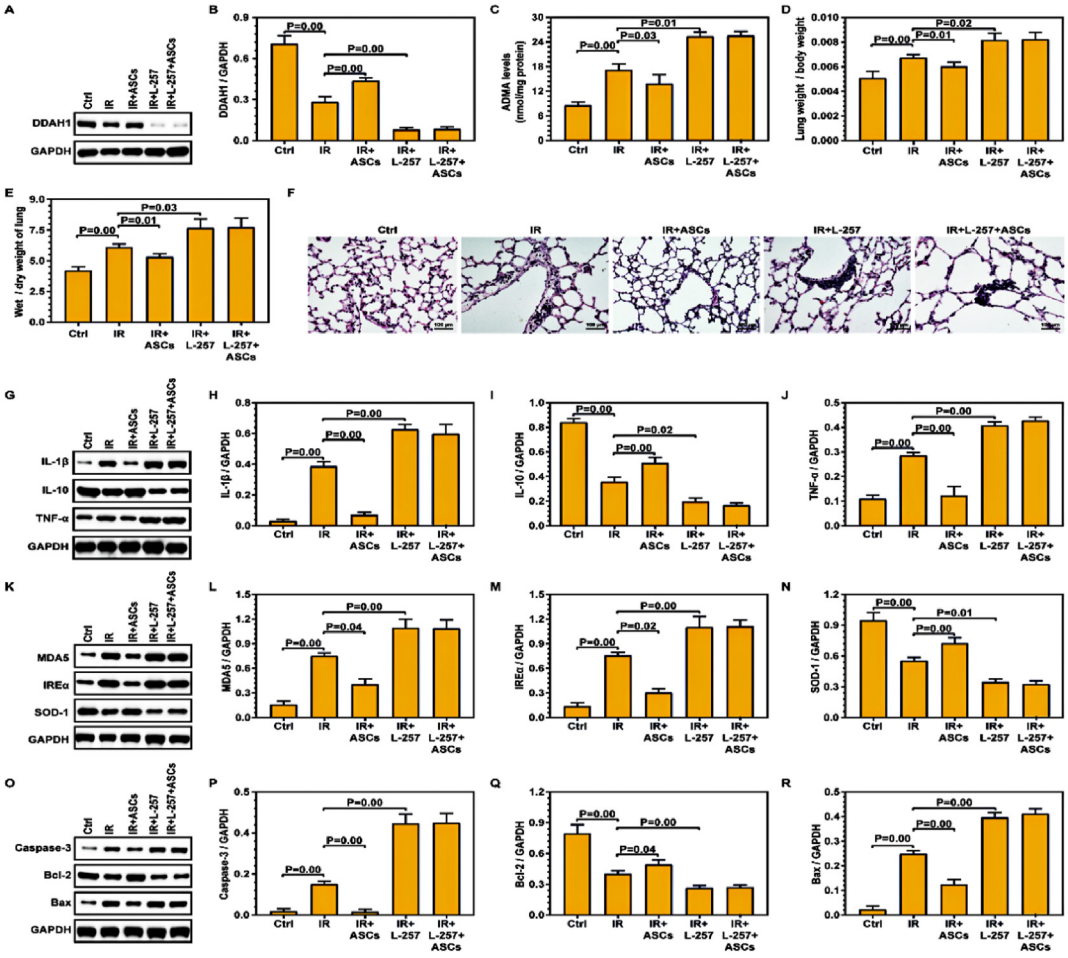

Fig. 8. L-257 pretreatment counteracted the protective effect of ASCs on lung injury induced by radiation exposure. (A–C) Representative Western blot images and quantitative analysis of DDAH1, ADMA and GAPDH. (D–E) Lung weight/body weight ratio and W/D ratio. (F) Representative histopathological lung images of rat. Scale bar = 100 μm. (G–J) Representative Western blot images and quantitative analysis of IL-1β, IL-10, TNF-α and GAPDH. (K–R) Representative Western blot images and quantitative analysis of MDA5, IREα, SOD-1, cleave caspase-3, Bcl-2, Bax and GAPDH. All experiments were repeated at least three times. Results are expressed as the mean ± SEM (n = 10 per roup).

minimal invasiveness and are less affected by the donor age. Autologous transplantation has no ethical controversies, and the cells have low immunogenicity. Our results showed that ASCs ameliorated IR-induced lung injury, reduced inflammatory cell infiltration and TNF-α, MPO, and IL-1β expression, and increased IL-10 expression. Caudal vein injection of ASCs maintains integrity of the lung epithelium, reduces serum levels of proinflammatory cytokines TNF-α, IL-1β, and IL-6, and increases anti-inflammatory cytokine IL-10, suggesting that ASCs attenuate radiation-induced acute lung injury through anti-inflammatory and anti-fibrosis signaling pathways [23,24]. Additionally, intratracheal injection of ASCs inhibits bleomycin-induced lung injury and pulmonary fibrosis in rats, and the mechanism involves changes in collagen turnover and inflammatory markers [25]. Similarly, the combination of ASCs and atto vastatin ameliorates amiodarone-induced lung injury in rats by reducing inflammation, apoptosis, and fibrosis in lungs [26]. Moreover, intratracheal injection of ASCs reduces the severity of pulmonary inflammation caused by *Staphylococcus aureus* infection and reduces the bacterial load and mortality of infected mice [27]. ASCs also have a protective effect against rat pneumonia caused by *Pseudomonas aeruginosa* by improving phagocytosis and bactericidal activity of macrophages through inhibition of PGE2 production [28]. These studies demonstrate that ASCs improve IR-induced lung injury by suppressing inflammation.

In the present study, ASCs significantly attenuated the increase in MDA5 and IRE-a expression and the decrease in SOD-1 expression caused by IR exposure. Furthermore, ASCs restored the decrease in Bcl-2 expression and the increase in Bax and cleaved caspase-3 expression caused by IR exposure. Takasaki et al. showed that coculture with ASCs protects neonatal rat ventricular myocytes from apoptosis caused by H_2O_2 treatment and significantly reduces oxidative stress under normoxic and hyperoxic conditions [29]. The protective effect of ASCs is related to increasing secretion of VEGF, IGF-1, and bFGF [30]. Additionally, extracellular vesicles secreted by ASCs attenuate PM2.5-induced apoptosis and necrosis of alveolar type II epithelial cells and improve lung injury and pulmonary fibrosis. Extracellular vesicles secreted by ASCs also suppress PM2.5-induced ROS levels and inflammatory responses [31]. In addition to anti-inflammatory and antioxidant functions, ASCs also reduce apoptosis and protect lungs from injury. Yang et al. found that ASCs combined with liraglutide attenuate acute lung injury by inhibiting PKA/β connexin and then inhibiting apoptotic signals [32]. In rats with chronic pancreatitis induced by dibutyltin dichloride, ASCs significantly reduce pancreatic injury and pancreatic cell apoptosis by regulating the expression of active

caspase-3, Bax, and Bcl-2 [33]. These data indicate that ASCs attenuate IR-induced lung injury, which may be related to their antioxidant and anti-apoptosis properties.

DDAH1 plays a crucial role in regulating angiogenesis, repairing vascular endothelial injury, and maintaining the NO signaling pathway by degrading ADMA. Furthermore, eNOS and eNOS-derived NO signaling play a vital role in the repair of vascular endothelial cells in acute lung injury and are fundamental factors in eliciting the hyperpermeability response [34]. eNOS regulates anti-proliferation and anti-apoptosis signaling pathways to maintain proper basal vasodilator tone of blood vessels during tissue repair [35]. Angiogenesis in eNOS-deficient mice is seriously impaired and vascular maturation and endothelial cell functions are regulated by eNOS during angiogenesis [36,37]. Our data demonstrated that ASCs significantly reversed high ADMA expression and low DDAH1 expression caused by IR exposure. Additionally, ASCs significantly increased eNOS expression and the NO concentration compared with the IR group. L-257 pretreatment offset the protective effect of ASCs against lung inflammation, oxidative stress, and apoptosis induced by IR exposure. These findings were consistent with a study by Gao et al. in which ASC treatment significantly increased eNOS expression in pulmonary microvascular endothelial cells and lung tissue [38]. ASCs also promoted the production of eNOS-derived NO and improved acute lung injury, suggesting that ASCs ameliorated acute lung injury through the eNOS/NO signaling pathway. This was also consistent with a study by Vilahur et al. in which ASC treatment significantly increased eNOS transcription and eNOS activity in myocardial infarcted pigs [39]. Additionally, DDAH1 knockout significantly aggravates pulmonary oxidative stress, pulmonary vascular remodeling, fibrosis, and pulmonary hypertension induced by monocrotaline in rats. DDAH1 knockout results in a significant increase in ADMA levels in plasma and lung tissue, and a significant decrease in eNOS levels in lung tissue. These results suggest that DDAH1 plays an essential role in reducing pulmonary oxidative stress and pulmonary hypertension induced by monocrotaline in rats [40]. Taken together, our results indicated that ASCs attenuated lung injury caused by Cold + IR exposure, and the mechanism may be closely related to the DDAH1/ADMA/eNOS signaling pathway.

5. Conclusion

In summary, our results suggest that IR exposure aggravates oxidative stress and apoptosis in lungs and promotes inflammatory cell infiltration. Furthermore, ASCs reduce IR-induced lung injury, whereas L-257 pretreatment counteracts the protective effect of ASCs against lung inflammation, oxidative stress, and apoptosis induced by IR exposure, suggesting that the mechanism is mediated through the DDAH1/ADMA/eNOS signaling pathway. IR-induced lung injury is a complex process involving many cytokines induced by ionizing radiation. There are few studies on ASCs for treatment of radiation-induced lung injury, most of which are based on animal models, and the clinical application remains to be analyzed further. However, with research progress, ASCs are expected to be a good seed cell type for the treatment of radiation-induced lung injury.

Ethics approval and consent to participate

The animal use protocol was approved by The Institutional Animal Care and Use Committee of General Hospital of Northern Theater Command (Shenyang, China), and the permit number is 2019W0128.

Funding

This study was supported by the Grant from National Natural Science Foundation of China (No. 31770908) and Key Program of National Natural Science Foundation of China (No. 82330100).

Author contributions

Quanwei Fu and Junye Liu designed experiments and wrote the manuscript. Yunen Liu revised and polished the manuscript. Qiaohui Gao and Shengyuan Jiao completed animal experiment, pathological experiment. Fei Da and Juan Guo completed molecular biology experiment and statistical analysis of data.

Availability of data and materials

The datasets used and/or analyzed during the current study are available from the corresponding author on reasonable request.

Patient consent for publication

Not applicable.

Declaration of competing interest

The authors declare that they have no known competing financial interests or personal relationships that could have appeared to influence the work reported in this paper.

Acknowledgements

Not applicable.

Appendix A. Supplementary data

Supplementary data to this article can be found online at https://doi.org/10.1016/j.reth.2024.04.001.

References

[1] Arroyo-Hernández M, Maldonado F, Lozano-Ruiz F, Muñoz-Montaño W, Nuñez-Baez M, Arrieta O. Radiation-induced lung injury: current evidence. BMC Pulm Med 2021;21(9).
[2] Xia P, Cao K, Hu X, Liu L, Yu DY, Dong SH, et al. K channel blocker glibenclamide prevents radiation-induced lung injury and inhibits radiation-induced apoptosis of vascular endothelial cells by increased Ca influx and subsequent PKC activation. Radiat Res 2020;193:171–85.
[3] Izumi Y, Nakashima T, Masuda T, Shioya S, Fukuhara K, Yamaguchi K, et al. Suplatast tosilate reduces radiation-induced lung injury in mice through suppression of oxidative stress. Free Radical Biol Med 2019;136:52–9.
[4] Hanania AN, Mainwaring W, Ghebre YT, Hanania NA, Ludwig M. Radiation-induced lung injury: assessment and management. Chest 2019;156:150–62.
[5] Aggarwal S, Gross CM, Kumar S, Dimitropoulou C, Sharma S, Gorshkov BA, et al. Dimethylarginine dimethylaminohydrolase II overexpression attenuates LPS-mediated lung leak in acute lung injury. Am J Respir Cell Mol Biol 2014;50:614–25.
[6] Liu X, Xu X, Shang R, Chen Y. Asymmetric dimethylarginine (ADMA) as an important risk factor for the increased cardiovascular diseases and heart failure in chronic kidney disease. Nitric Oxide 2018;78:113–20.
[7] López V, Moraga FA, Llanos AJ, Ebensperge r G, Taborda MI, Uribe E. Plasmatic concentrations of ADMA and homocystein in llama and regulation of arginase type II: an animal resistent to the development of pulmonary hypertension induced by hypoxia. Front Physiol 2018;9:606.
[8] He H, Qiao Y, Zhou Q, Wang ZQ, Chen XP, Liu D, et al. Iron overload damages the endothelial mitochondria the ROS/ADMA/DDAHII/eNOS/NO pathway. Oxid Med Cell Longev 2019;2019:2340392.
[9] Sun GC, Wong TY, Chen HH, Ho CY, Yeh TC, Ho WY, et al. Angiotensin II inhibits DDAH1-nNOS signaling via AT1R and μOR dimerization to modulate blood pressure control in the central nervous system. Clin Sci 2019;133:2401–13.
[10] Zhao C, Li T, Han B, Yue WH, Shi LL, Wang HY, et al. DDAH1 deficiency promotes intracellular oxidative stress and cell apoptosis via a miR-21-

dependent pathway in mouse embryonic fibroblasts. Free Radic Biol Med 2016;92:50–60.
[11] Zölner J, Lambden S, Nasri NM, Johnson MR, Leiper J. Inhibition of dimethylarginine dimethylaminohydrolase 1 improves the outcome of sepsis in pregnant mice. Shock 2020;54:498–506.
[12] Lee MY, Tsai KB, Hsu JH, Shin SJ, Wu JR, Yeh JL. Liraglutide prevents and reverses monocrotaline-induced pulmonary arterial hypertension by suppressing ET-1 and enhancing eNOS/sGC/PKG pathways. Sci Rep 2016;6:31788.
[13] Duan MX, Zhou H, Wu QQ, Liu C, Xiao Y, Deng W, et al. Andrographolide protects against HG-induced inflammation, apoptosis, migration, and impairment of angiogenesis via PI3K/AKT-eNOS signalling in HUVECs. Mediat Inflamm 2019;2019:6168340.
[14] Feng Y, Zhou L, Peng Y, Yang YC, Fan TY, Jiang X, et al. The role of miR-326 in adipogenic differentiation of human adipose-derived stem cells by targeting C/EBPα in vitro. Anat Rec 2020;303:2054–60.
[15] Feng J, Hu W, Fanai ML, Zhu SQ, Wang J, Cai JR, et al. Mechanical process prior to cryopreservation of lipoaspirates maintains extracellular matrix integrity and cell viability: evaluation of the retention and regenerative potential of cryopreserved fat-derived product after fat grafting. Stem Cell Res Ther 2019;10:283.
[16] Panina YA, Yakimov AS, Komleva YK, Morgun AV, Lopatina OL, Malinovskaya NA, et al. Plasticity of adipose tissue-derived stem cells and regulation of angiogenesis. Front Physiol 2018;9:1656.
[17] Pers YM, Quentin J, Feirreira R, Espinoza F, Abdellaou N, Erkilic N, et al. Injection of adipose-derived stromal cells in the knee of patients with severe osteoarthritis has a systemic effect and promotes an anti-inflammatory phenotype of circulating immune cells. Theranostics 2018;8:5519–28.
[18] Pak J, Lee JH, Pak N, Pak Y, Park W, Jeon J, et al. Cartilage regeneration in humans with adipose tissue-derived stem cells and adipose stromal vascular fraction cells: updated status. Int J Mol Sci 2018:19.
[19] Hoke NN, Salloum FN, Kass DA, Das A, Kukreja RC. Preconditioning by phosphodiesterase-5 inhibition improves therapeutic efficacy of adipose-derived stem cells following myocardial infarction in mice. Stem Cell 2012;30:326–35.
[20] Blokzijl F, de Ligt J, Jager M, Sasselli V, Roerink S, Sasaki N, et al. Tissue-specific mutation accumulation in human adult stem cells during life. Nature 2016;538:260–4.
[21] Chen CC, Hsu LW, Nakano T, Huang KT, Chen KD, Lai CY, et al. DHL-HisZn, a novel antioxidant, enhances adipogenic differentiation and antioxidative response in adipose-derived stem cells. Biomed Pharmacother 2016;84:1601–9.
[22] Ansari MY, Ahmad N, Haqqi TM. Butein activates autophagy through AMPK/TSC2/ULK1/mTOR pathway to inhibit IL-6 expression in IL-1beta stimulated human chondrocytes. Cell Physiol Biochem 2018;49(I).
[23] Ihara K, Fukuda S, Enkhtaivan B, Trujillo R, Perez-Bello D, Nelson C, et al. Adipose-derived stem cells attenuate pulmonary microvascular hyperpermeability after smoke inhalation. PLoS One 2017;12:e0185937.
[24] Zhang S, Danchuk SD, Imhof KM, Semon JA, Scruggs BA, Bonvillain RW, et al. Comparison of the therapeutic effects of human and mouse adipose-derived stem cells in a murine model of lipopolysaccharide-induced acute lung injury. Stem Cell Res Ther 2013;4:13.
[25] Tashiro J, Elliot SJ, Gerth DJ, Xia XM, Pereira-Simon S, Choi R, et al. Therapeutic benefits of young, but not old, adipose-derived mesenchymal stem cells in a chronic mouse model of bleomycin-induced pulmonary fibrosis. Transl Res 2015;166:554–67.
[26] Radwan SM, Ghoneim D, Salem M, Saeed M, Saleh Y, Elhamy M, et al. Adipose tissue-derived mesenchymal stem cells protect against amiodarone-induced lung injury in rats. Appl Biochem Biotechnol 2020;191:1027–41.
[27] Sun CK, Leu S, Hsu SY, Zhen YY, Chang LT, Tsai CY, et al. Mixed serum-deprived and normal adipose-derived mesenchymal stem cells against acute lung ischemia-reperfusion injury in rats. Am J Transl Res 2015;7:209–31.
[28] Mao YX, Xu JF, Seeley EJ, Tang XD, Xu LL, Zhu YG, et al. Adipose tissue-derived mesenchymal stem cells attenuate pulmonary infection caused by Pseudomonas aeruginosa via inhibiting overproduction of prostaglandin E2. Stem Cell 2015;33:2331–42.
[29] Takasaki Y, Watanabe M, Yukawa H, Sabarudin A, Inagaki K, Kaji N, et al. Estimation of the distribution of intravenously injected adipose tissue-derived stem cells labeled with quantum dots in mice organs through the determination of their metallic components by ICPMS. Anal Chem 2011;83:8252–8.
[30] Lin Y, Li X, Fan C, Yang F, Hao DJ, Ge WJ, et al. Cardioprotective effects of rat adipose-derived stem cells differ under normoxic/physioxic conditions and are associated with paracrine factor secretion. Int J Mol Med 2020;45:1591–600.
[31] Gao Y, Sun J, Dong C, Zhao M, Hu Y, Jin F. Extracellular vesicles derived from adipose mesenchymal stem cells alleviate pm2.5-induced lung injury and pulmonary fibrosis. Med Sci Monit 2020;26:e922782.
[32] Yang X, Ma X, Don O, Song YL, Chen XY, Liu JW, et al. Mesenchymal stem cells combined with liraglutide relieve acute lung injury through apoptotic signaling restrained by PKA/β-catenin. Stem Cell Res Ther 2020;11.
[33] Xu X, Yu H, Sun L, Zheng CL, Shan YF, Zhou ZX, et al. Adipose-derived mesenchymal stem cells ameliorate dibutyltin dichloride-induced chronic pancreatitis by inhibiting the PI3K/AKT/mTOR signaling pathway. Mol Med Rep 2020;21:1833–40.
[34] Bao XC, Mao AR, Fang YQ, Fan YH, Wang FF, Ma J, et al. Simvastatin decreases hyperbaric oxygen-induced acute lung injury by upregulating eNOS. Am J Physiol Lung Cell Mol Physiol 2018;314:L287–97.
[35] Kamel NM, Abd El, Fattah MA, El-Abhar HS, Abdallah DM. Novel repair mechanisms in a renal ischaemia/reperfusion model: subsequent saxagliptin treatment modulates the pro-angiogenic GLP-1/cAMP/VEGF, ANP/eNOS/NO, SDF-1α/CXCR4, and Kim-1/STAT3/HIF-1α/VEGF/eNOS pathways. Eur J Pharmacol 2019;861:172620.
[36] Ha JM, Jin SY, Lee HS, Shin HK, Lee DH, Song SH, et al. Regulation of retinal angiogenesis by endothelial nitric oxide synthase signaling pathway. Korean J Physiol Pharmacol 2016;20:533–8.
[37] Katusic ZS. Therapeutic angiogenesis: new indication for endothelial NO synthase gene transfer. Arterioscler Thromb Vasc Biol 2002;22:1254–5.
[38] Gao P, Yang X, Mungur L, Kampo S, Wen Q. Adipose tissue-derived stem cells attenuate acute lung injury through eNOS and eNOS-derived NO. Int J Mol Med 2013;31:1313–8.
[39] Vilahur G, Oñate B, Cubedo J, Béjar MT, Arderiu G, Peña E, et al. Allogenic adipose-derived stem cell therapy overcomes ischemia-induced microvessel rarefaction in the myocardium: systems biology study. Stem Cell Res Ther 2017;8(52).
[40] Wang D, Li H, Weir EK, Xu Y, Xu D, Chen Y. Dimethylarginine dimethylaminohydrolase 1 deficiency aggravates monocrotaline-induced pulmonary oxidative stress, pulmonary arterial hypertension and right heart failure in rats. Int J Cardiol 2019;295:14–20.